Microstructure and Texture Evolution During Sub-Transus Thermo-Mechanical Processing of Ti-6Al-4V-0.1B Alloy: Part II. Static Annealing in ($\alpha + \beta$) Regime

SHIBAYAN ROY, S. KARANTH, and SATYAM SUWAS

The first part of this study describes the evolution of microstructure and texture in Ti-6Al-4V-0.1B alloy during sub-transus rolling vis-à-vis the control alloy Ti-6Al-4V. In the second part, the static annealing response of the two alloys at self-same conditions is compared and the principal micromechanisms are analyzed. Faster globularization kinetics has been observed in the Ti-6Al-4V-0.1B alloy for equivalent annealing conditions. This is primarily attributed to the α colonies, which leads to easy boundary splitting *via* multiple slip activation in this alloy. The other mechanisms facilitating lamellar to equiaxed morphological transformations, *e.g.*, termination migration and cylinderization, also start early in the boron-modified alloy due to small α colony size, small aspect ratio of the α lamellae, and the presence of TiB particles in the microstructure. Both the alloys exhibit weakening of basal fiber (ND||$\langle 0001 \rangle$) and strengthening of prism fiber (RD||$\langle 10\bar{1}0 \rangle$) upon annealing. A close proximity between the orientations of fully globularized primary α and secondary α phases during $\alpha \rightarrow \beta \rightarrow \alpha$ transformation has accounted for such a texture modification.

DOI: 10.1007/s11661-013-1673-3

I. INTRODUCTION

IN the first part of this study, microstructure and texture development for Ti-6Al-4V-0.1B alloy have been presented in comparison with a control Ti-6Al-4V alloy.[1] The second part addresses the static annealing response of Ti-6Al-4V-0.1B alloy vis-à-vis the control Ti-6Al-4V alloy. Among the various rolled materials, the low temperature deformed specimens of the two alloys have been preferred for the present study in order to distinguish the effect of static annealing from the dynamic globularization during high temperature rolling. In the processing of titanium and its alloys, the conversion from lamellar to equiaxed morphology is of great importance since superior strength and ductility are well balanced for an equiaxed microstructure. Such microstructural engineering is generally accomplished by sub β-transus deformation followed by post-deformation sub-transus annealing.[2–4]

While the static annealing behavior of the deformed Ti-6Al-4V alloy is well documented and micromechanisms for microstructural conversion are well understood,[5–9] no such study has been reported for the boron-modified Ti-6Al-4V alloy. A comprehensive understanding of microstructure and texture evolution is, therefore, lacking for this alloy system. In the present work, a systematic study has been carried out pertaining to the evolution of microstructure and texture after annealing of the warm-rolled [973 K (700 °C) up to 90 pct thickness reduction] Ti-6Al-4V-0.1B alloy. A similar experiment has been performed on the Ti-6Al-4V control alloy. The effect of boron is finally separated from the similarities and differences in the microstructure and texture of the two alloys in self-same conditions.

II. EXPERIMENTAL PROCEDURE

A. *Material*

The details of the starting alloy compositions and cast ingot specifications are provided in Section II–A of Part I. For this part of the investigation, the warm-rolled specimens of Ti-6Al-4V and Ti-6Al-4V-0.1B (hereafter referred to as Ti64 and Ti64 + B, respectively), namely the ones rolled at 973 K (700 °C) up to a thickness reduction of 90 pct, were chosen for the subsequent annealing experiments.

B. *Annealing Experiment*

The annealing experiment involve heat treatment of smaller coupons (20 mm × 5 mm × 1 mm) prepared from the sub-transus rolled strips of the two alloys. The specimens were isothermally annealed at 1173 K (900 °C) for 15, 30, 45, 60, 75, and 90 minutes in the case of Ti64 and 15, 30, 45, and 60 minutes for Ti64 + B with argon atmosphere. After the respective heat treatments, the specimens were air cooled to room temperature in approximately 30 seconds. A forced convection cooling was used to cool the specimens *via* cold air blowing immediately after

SHIBAYAN ROY, formerly Ph.D. Student with the Department of Materials Engineering, Indian Institute of Science, Bangalore, India, is now Post-doctoral Researcher with the Institut für Werkstoffwissenschaft und Werkstofftechnik, Chemnitz University of Technology, Chemnitz, Germany. S. KARANTH, Summer Trainee, and SATYAM SUWAS, Associate Professor, are with the Department of Materials Engineering, Indian Institute of Science, Bangalore, India. Contact e-mail: satyamsuwas@materials.iisc.ernet.in

Manuscript submitted May 31, 2012.
Article published online March 20, 2013

removing from the furnace. Fast cooling is preferred in order to avoid changes in the microstructure during cooling that prevailed at the actual annealing condition. Such changes primarily include coarsening of equiaxed primary α grains by Ostwald ripening which may adversely affect the room temperature characterization of microstructure and texture.[9] In addition, the formation of secondary ($\alpha_s + \beta$) colonies during cooling strongly depends on the cooling rate.[7] In order to facilitate image analysis to calculate prior β phase fraction at annealing condition, a faster cooling rate is essential so that the α_s phase forms with sufficient vanadium super-saturation and produces enough contrast in the BSE micrographs.

C. *Microstructural Characterization by SEM and EBSD*

Microstructural observations (SEM and EBSD) were made on the cross-sectional ND-RD plane (long transverse plane) of the annealed specimens. The details of specimen surface preparation for SEM and EBSD are described in Sections II–B and II–C of Part I, respectively. The parameters of the EBSD scans (*e.g.*, scanned area, step size, *etc.*) are given in Table I. The BSE micrographs were analyzed to calculate the volume fraction of primary α phase in the room temperature microstructure. The details of the image analysis procedure to separate primary (α_p) and secondary α (α_s) plus β phases in the microstructure are described in Section II–C of Part I. The primary α phase remains stable at annealing condition and transforms back to room temperature without change. The secondary α, plus the retained β at room temperature, is transformed from the β phase which was present at the annealing condition. If a correct intensity threshold is chosen, primary α (dark contrast) can be separated from prior β (bright contrast) in the BSE micrographs. The volume fraction of these two phases can be calculated as

$$\text{Primary } \alpha(\%) = \frac{\text{Area with dark contrast in BSE micrograph}}{\text{Total area in BSE micrograph}} * 100$$

$$\text{Prior } \beta\,(\%)\ \textit{i.e.},\ \text{secondary } \alpha \text{ plus retained } \beta = \frac{\text{Area with bright contrast in BSE micrograph}}{\text{Total area in BSE micrograph}} * 100$$

In the EBSD derived orientation maps, the separation between primary and secondary α phase is carried out based on 'image quality' criterion described in Section II–D of part I. Finally, compositional analysis was performed on the electro-polished surface (ND-RD plane) of Ti64 + B alloy annealed up to 60 minutes using a field emission electron probe micro-analyser (FEG-EPMA)* in wavelength dispersive (WDS) mode.

*JXA-8530F, JEOL, Japan.

The length and thickness measurements of the primary α phase in the annealed specimens were carried out by the linear intercept method using several horizontal (for length) and vertical (for thickness) test lines to obtain statistically averaged values with 95 pct confidence level. It was, however, not possible to carry out the measurement on the as-rolled specimens of the two alloys as well as on certain annealed specimens (15 and 30 minutes) of the Ti64 alloy. For the rolled specimens, the α colonies are either straightened along the RD or they are kinked, which makes length measurement conditions difficult. The thickness measurement is similarly restricted due to the difficulty to demarcate the α/β interphase at several places. The measurement conditions are slightly better after 15 and 30 minutes of annealing for the Ti64 alloy, although not suitable enough to report the absolute values unambiguously. The measured average section length (l_{avg}) and thickness (t_{avg}) values were corrected using the Fullman correction factor[10] described as

$$(l_{avg})_{true} = \frac{p}{2} \times (l_{avg})_{measured} \quad \text{and}$$

$$(t_{avg})_{true} = \frac{p}{4} \times (t_{avg})_{measured}$$

Edge grains were excluded from the measurement scheme, and aspect ratio of α lamellae was calculated as $(l_{avg})_{true}/(t_{avg})_{true}$. The globularized α phase was separated from the total primary α phase using the aspect ratio criterion that distinguishes the globularized α grains as the one with an aspect ratio <2.[11] It is to be noted that the globularized α phase is a part of the total primary α phase and should not be considered separately. Globularized α fraction in the microstructure is calculated as

$$\text{Globularized } \alpha\ (\%) = \frac{\text{Area with dark contrast and aspect ratio} < 2}{\text{Total area in BSE micrograph}}.$$

Table I. Details of EBSD Scans for the Two Alloys After Different Annealing Durations

Alloy	Annealing Time (min)	Scan Area (X μm × Y μm)	Step Size (nm)
Ti64	30	90 × 75	220
	60	75 × 75	200
	90	65 × 70	100
Ti64 + B	15	100 × 75	250
	30	80 × 80	200
	60	75 × 75	100

D. *Texture Characterization*

The experimental details of bulk texture measurement by the X-ray diffraction technique are presented in Section II–D of Part I. In this part, the bulk texture was measured from the mid thickness region of the RD-TD plane for 60 and 90 minutes annealed specimens of the Ti64 and 30 and 60 minutes for the Ti64 + B alloy.

III. RESULTS

The microstructure and texture of low temperature rolled specimens for the two alloys (Ti64 and Ti64 + B)

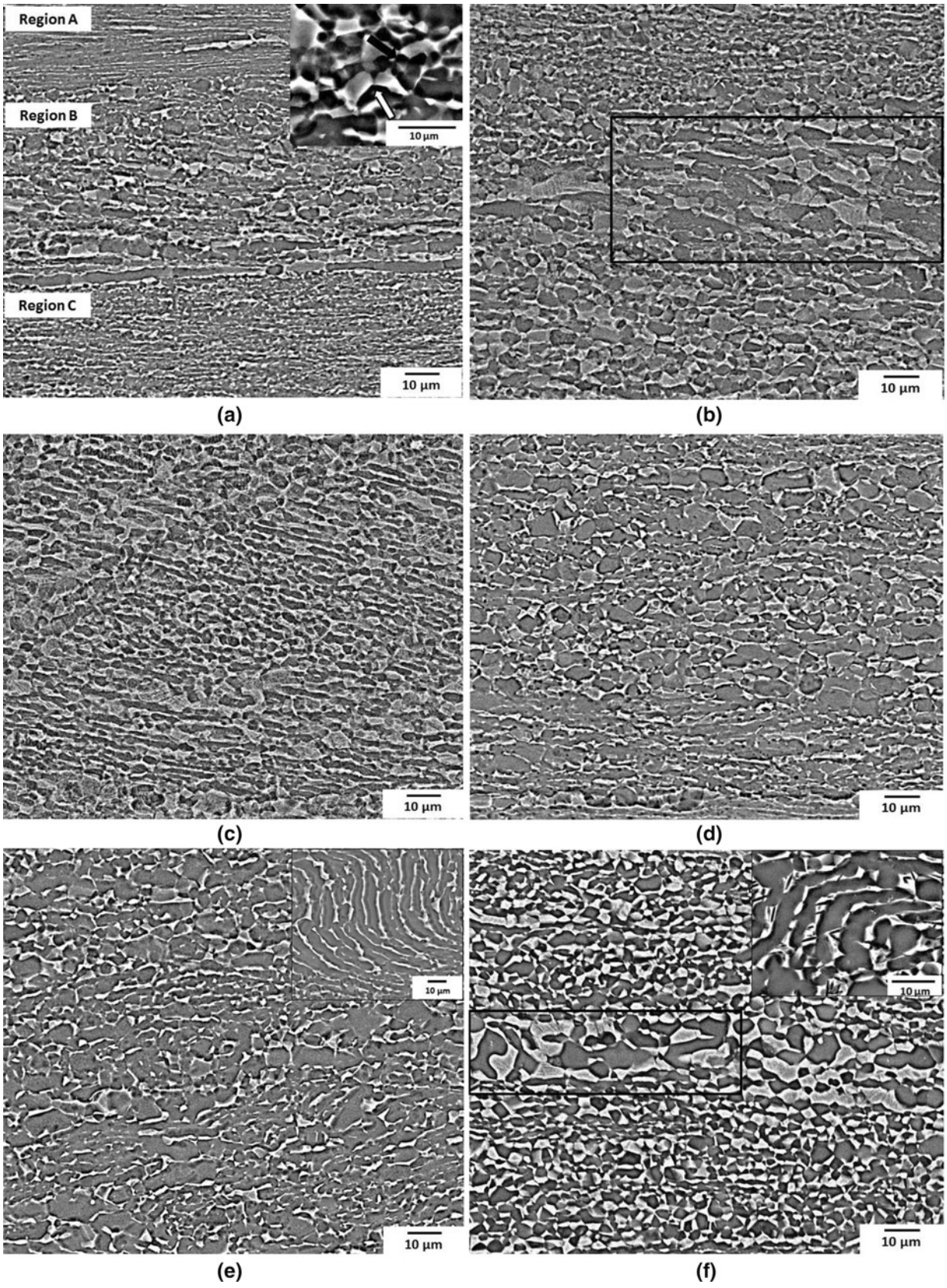

Fig. 1—SEM micrographs (BSE mode) showing microstructures for Ti64 alloy after (*a*) 15 min, (*b*) 30 min, (*c*) 45 min, (*d*) 60 min, (*e*) 75 min, and (*f*) 90 min of annealing. Insets (a), (e), and (f) are BSE micrographs showing microstructures at higher magnifications after 15, 75, and 90 min of annealing, respectively. Original rolling direction is horizontal (→) for all the micrographs. In these micrographs, the darker contrast represents α phase, while the brighter contrast represents β phase.

are described in Sections III–A and III–B, respectively, of Part I.

A. *Microstructure of Ti64 After Annealing*

The microstructure of the Ti64 alloy after annealing for 15 minutes shows different features at three regions marked as A, B, and C in Figure 1(a). In the middle region B, several equiaxed α_p grains can be seen surrounded by prior β regions, which indicate globularization. Limited penetration of the β phase into the α lamellae is also observed at certain places in this region. At the bottom, such equiaxed α_p grains are not seen in region C, although the β phase is mostly broken into small particles and penetrates into the α lamellae at a few locations (marked by white arrow in Figure 1(a) inset). At certain locations, the α phase also penetrates into the β lamellae and forms a continuous network (marked by black arrow in Figure 1(a) inset). This indicates the initiation of globularization.[8] The topmost region A shows neither equiaxed α_p grains nor broken β particles, which indicates that globularization does not even initiate for the α lamellae in this region.

After 30 minutes of annealing, many of the α lamellae appear globularized in the microstructure, although the equiaxed α_p grains show large size variations (Figure 1(b)). A few α lamellae are also characterized by high aspect ratio (in the marked region of the micrograph). These are possibly the remnants of the initial α lamella, which are yet to globularize. Globularization continues in the microstructure after 45 minutes of annealing in most of the RD-aligned α lamellae (Figure 1(c)). The extent of globularization progressively increases with annealing time and after 60 minutes, the β phase penetrates through most of the α lamellae at different locations (Figure 1(d)). After 75 minutes, the straight α lamellae are almost completely divided into equiaxed α_p grains and surrounded by the prior β phase (Figure 1(e)). The kinked α colonies initially present in the rolled specimens, however, retain their morphology without showing any sign of globularization (Figure 1(e) inset). The β phase is also divided into smaller fragments by α phase penetration at a few places in the straight as well as within the kinked α colonies. On further annealing for 90 minutes, the α lamellae that are initially aligned along the RD completely transform to equiaxed α_p grains (Figure 1(f)), except a few locations where the globularization process is not yet over (regions marked in the middle of the micrograph). The kinked α lamellae also lead to the formation of equiaxed α_p grains at various locations (Figure 1(f) inset). The prior β phase remains largely confined as separate islands between the equiaxed α_p grains in both the straight and kinked α lamellae.

B. *Microstructure of Ti64 + B After Annealing*

In the initial stages of annealing (15 and 30 minutes), the microstructure of Ti64 + B alloy consists of regions where straight α lamellae (initially aligned along RD) contain fully equiaxed α_p grains and remnants of high aspect ratio α lamellae at a few places (Figures 2(a) and (b)). The microstructure after 15 minutes of annealing also contains regions (at the middle of the micrograph) which were initially kinked and partly globularized (marked in the micrograph). The β phase gets fragmented into smaller particles near the kinked α lamellae. Incomplete β phase penetration (through α lamellae) and β phase fragmentation are also observed for straight α lamellae at certain locations in the microstructure. After 30 minutes, a large number of α lamellae get divided into equiaxed α_p grains, while the β phase remains as isolated islands in the microstructure. After 45 and 60 minutes of annealing, nearly equiaxed α_p grains form in most of the α lamellae (Figures 2(c) and (d)). In some regions, the remnants of high aspect ratio α lamellae are still prevalent, showing partial β phase penetrations, preferably in the vicinity of TiB particles (indicated in Figure 2(c) inset). The equiaxed α_p grains show coarsening after 60 minutes of annealing. One such coarse α_p grain is shown with an arrow in the inset of Figure 2(d).

C. *Analysis of Microstructural Features*

As shown in Table II, the amount of secondary α markedly increases on annealing from the as-rolled condition, while primary α content remains almost constant with annealing time for both the alloys. The amount of secondary α at the annealing temperature of 1173 K (900 °C) is higher in the Ti64 + B alloy as compared to the Ti64 alloy. The variation in the aspect ratio of α_p grains (Figure 3(a)) and the globularized fraction of the total primary α phase (Figure 3(b)) with annealing time indicate the differences in the annealing kinetics for the two alloys. The aspect ratio decreases almost linearly from ~4 after 30 minutes to ~3 after 90 minutes of annealing for the Ti64 alloy. In the case of the Ti64 + B alloy, the aspect ratio drops from ~3 after 15 minutes to ~2.5 after 30 minutes of annealing and remains constant henceforth. For the same annealing period (*e.g.*, after 30, 45 or 60 minutes), the aspect ratio of α_p grains is lower for Ti64 + B compared to Ti64 alloy. The amount of globularized α_p grains in the microstructure increases almost linearly with annealing time for both the alloys. The globularization kinetics is, however, faster for the Ti64 + B alloy with the fraction of globularized α_p grains increasing from ~25 pct after 15 minutes to ~45 pct after 60 minutes. In the case of the Ti64 alloy, only ~18 pct and ~30 pct of α_p phase globularize after 30 and 90 minutes, respectively. Overall, the amount of globularized α_p grains for the Ti64 alloy is always lower than the Ti64 + B alloy for any given annealing duration.

D. *Texture Evolution*

Relevant 3D ODFs after annealing show intensity distribution along characteristic texture fibers (basal fiber with ND$\|\langle 0001\rangle$ and prism fiber with RD$\|\langle 10\bar{1}0\rangle$) for the two alloys (Figure 4). The maximum intensity along these fibers corresponds to discrete texture components which are listed in Table III. For the Ti64 alloy, the characteristics of rolling texture including the texture components and intensity of the texture fibers remain preserved after 60 minutes of annealing (Figure 4(a)). After 90 minutes, the basal fiber significantly weakens

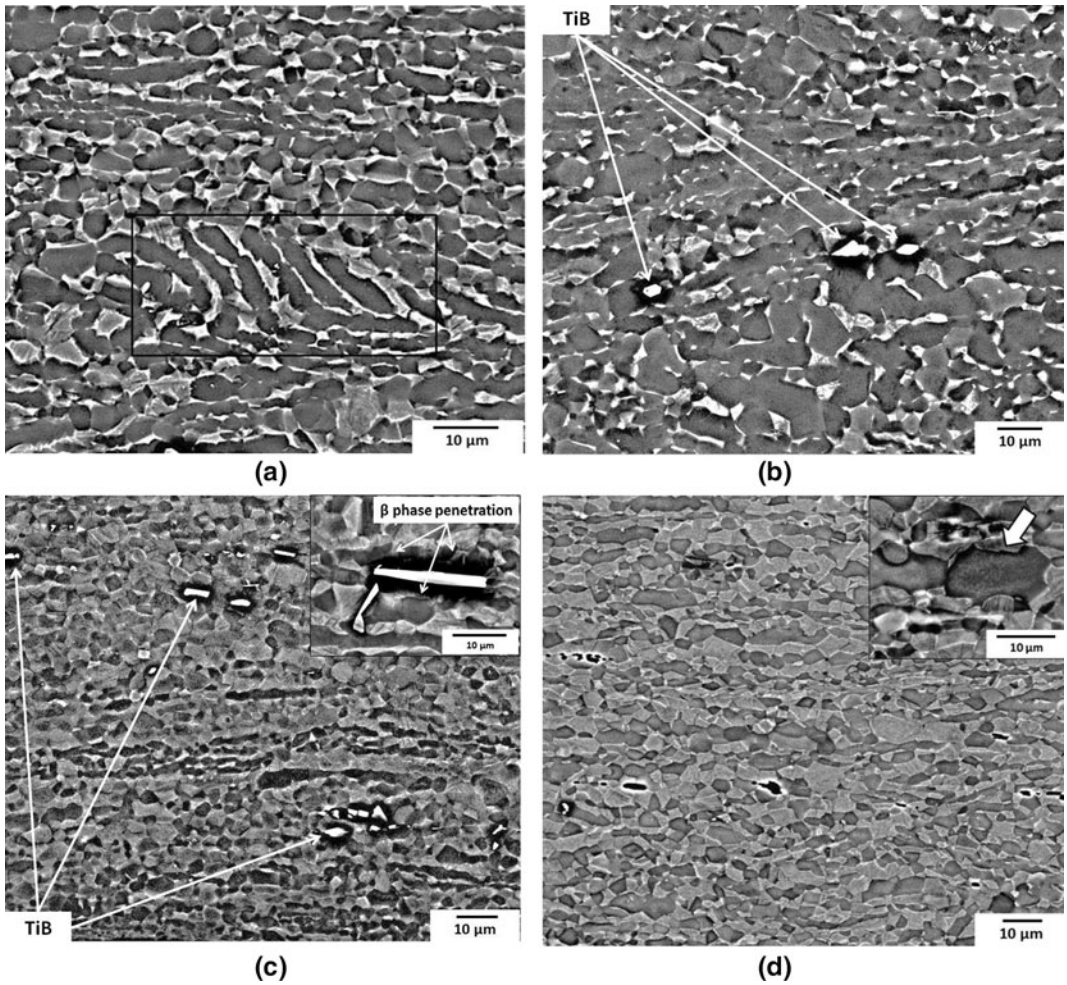

Fig. 2—SEM micrographs (BSE mode) showing microstructures for Ti64 + B alloy after (*a*) 15 min, (*b*) 30 min, (*c*) 45, and (*d*) 60 min of annealing. Original rolling direction is horizontal (→) for all the micrographs. *Insets* (c) and (d) are BSE micrographs showing microstructures at higher magnifications after 45 and 60 min of annealing, respectively. In these micrographs, the darker contrast represents α phase, while the brighter contrast represents β phase. The TiB particles are indicated in (b) and (c) and can be identified in other micrographs from the bright, white contrast. The arrow in (d) inset indicates the presence of a coarse primary α grain in the microstructure after 60 min of annealing.

Table II. Volume Fraction of Primary α and Globularized α as Measured from Image Analysis of BSE Micrographs at Various Annealing Durations for the Two Alloys

Alloy	Annealing Time (min)	Primary α (pct)	Globularized α (pct)	Prior β, *i.e.*, Secondary α Plus Retained β (pct)
Ti64	0	84 ± 2	—	16 ± 2
	15	68 ± 2.6	—	32 ± 2.6
	30	62 ± 2.4	—	38 ± 2.4
	45	64.5 ± 2.9	18 ± 0.5	35.5 ± 2.9
	60	67.4 ± 3.7	20.5 ± 0.5	32.6 ± 3.7
	75	66.4 ± 3.3	24 ± 1.5	33.6 ± 3.3
	90	66.8 ± 3.7	30.3 ± 2.5	33.2 ± 3.7
Ti64 + B	0	78.5 ± 3	—	21.5 ± 3
	15	62.6 ± 2.2	25.8 ± 1.4	37.4 ± 2.2
	30	61.5 ± 4.7	31.4 ± 0.5	38.5 ± 4.7
	45	58 ± 3.8	36 ± 1	42 ± 3.8
	60	61 ± 3	44.8 ± 1.4	39 ± 3

and becomes incomplete in the φ_1 direction (Figure 4(b)). For the Ti64 + B alloy, weakening of the basal fiber is observed after 30 minutes and continues up to 60 minutes of annealing (Figures 4(c) and (d)). The prism fiber, on the other hand, appears strong and complete in the Φ direction for both the alloys at all the annealing durations. The main component on the prism fiber occurs as $(1\bar{2}1l)[10\bar{1}0]$ for both the alloys irrespective of annealing

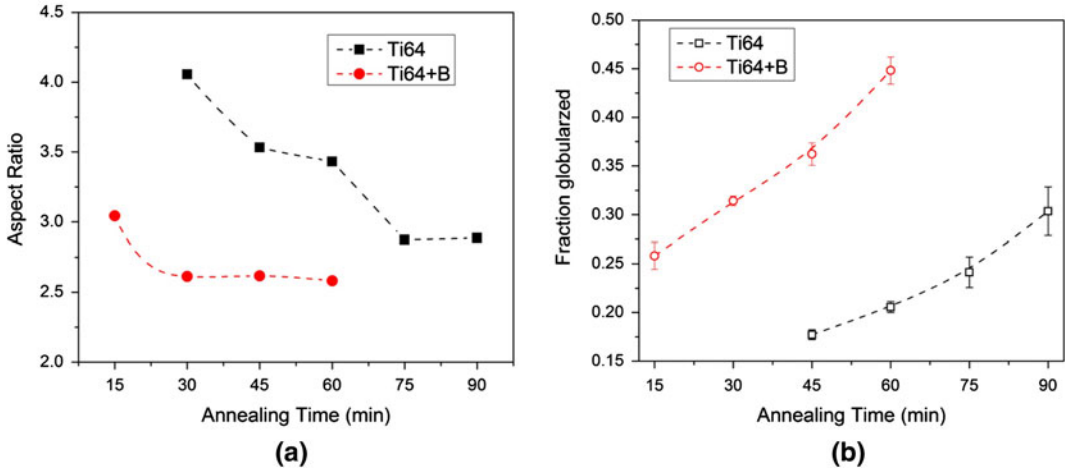

Fig. 3—Variation in (*a*) primary α grain aspect ratio and (*b*) globularized fraction of primary α with annealing time for the two alloys (For interpretation of the references to color in this figure legend, the reader is referred to the web version of this article).

time (Table III), wherein only the last index "*l*" of planes parallel to the rolling plane changes with annealing time, while the direction parallel to the rolling direction remains always fixed. The main component in the basal fiber similarly appears as $(10\bar{1}l)[uvt1]$, wherein all the indices of the direction parallel to the rolling direction vary with annealing time (Table III).

It is to be noted that the components in the basal fiber apparently do not belong to the definition of ND||⟨0001⟩. There are two reasons for this observed discrepancy; firstly, the true basal fiber with ND||⟨0001⟩ is located only within $\Phi = 0$ deg and $\varphi_1 = 0$–90 deg locations.[12] The actual basal fiber extends in the Φ direction up to ~10 to 20 deg, which is characteristics of the texture fibers for hexagonal metals like titanium.[13–19] Secondly, the basal fiber at times completely shifts in the Φ direction up to 20 to 30 deg and becomes a fiber with $ND||\langle hkil\rangle$ where all the indices of the planes parallel to the rolling plane vary along the φ_1 direction.[19] The basal fiber, in the real sense, should be defined as the texture fiber that runs in the Euler space parallel to φ_1 direction rather than being defined by ND||⟨0001⟩. Under both the situations, the texture component that corresponds to the intensity maxima in the basal fiber most likely becomes $(10\bar{1}l)[uvt1]$.

The $f(g)_{max}$ of the basal and prism texture fibers is presented in Table IV. In the as-rolled condition, the basal fiber is stronger than the prism fiber for both the alloys. In the case of the Ti64 alloy, the strength of the basal fiber decreases continuously up to 90 minutes. The prism fiber, however, strengthens significantly after 60 minutes and remains almost constant up to 90 minutes. For the alloy Ti64 + B, weakening of basal fiber and strengthening of prism fiber occur after 30 minutes and remain almost constant up to 60 minutes.

IV. DISCUSSION

A. *Microstructural Differences Between Two Alloys on Annealing*

From the trends in microstructural development, it is clear that the globularization kinetics is faster for the Ti64 + B compared to the Ti64. During static annealing of titanium alloys with a colony microstructure, the lamellar morphology of the α phase transforms to an equiaxed one by one or a combination of mechanisms like Rayleigh perturbation instability, direct cylinderization, edge spheroidization, boundary splitting (boundary formation followed by thermal grooving), termination migration, fault migration, *etc*.[23–29] Out of these, dynamic globularization mainly proceeds by boundary formation and thermal grooving which are discussed in Section IV–A–4 of Part I. Static globularization, on the other hand, is primarily controlled by both boundary splitting and termination migration.[5–9] In addition, when the aspect ratio of the α lamellae sufficiently decreases below a certain critical limit due to termination migration, globularization can occur by direct cylinderization.[24,26] Recall that the cast microstructure of the Ti64 + B alloy differs from that of the Ti64 by the presence of TiB particles, smaller aspect ratio of the α lamellae (larger thickness), and smaller α colony size.[19–22]

1. *Boundary formation*

As discussed in Section IV–A–4 of Part I, the boundary formation inside the deformed α lamellae during rolling primarily depends on its orientation with respect to the principal directions. A similar argument holds true during annealing wherein recovery-assisted boundary formation is controlled by the initial α colony orientation. For example, simultaneous basal and prism slip for orientation 2 or 3 in Table V (reference color violet/magenta/yellow) leads to dislocation substructure formation during prior rolling and stable dislocation walls in the α lamellae during annealing.[29–32] Such an α colony in Figures 5 and 6 indeed shows low angle transverse boundaries after annealing. Orientation 1 in Table V (reference color red in the IPF maps) generally leads to strict prism slip during rolling.[32] Transverse low angle boundaries do not form in such α colonies on annealing since only prism slip produces unstable dislocation walls in the thickness direction of any α lamellae (Figure 6(b)).[29] Orientations 4 and 5 in Table V (reference color blue/green), on the other hand, do not

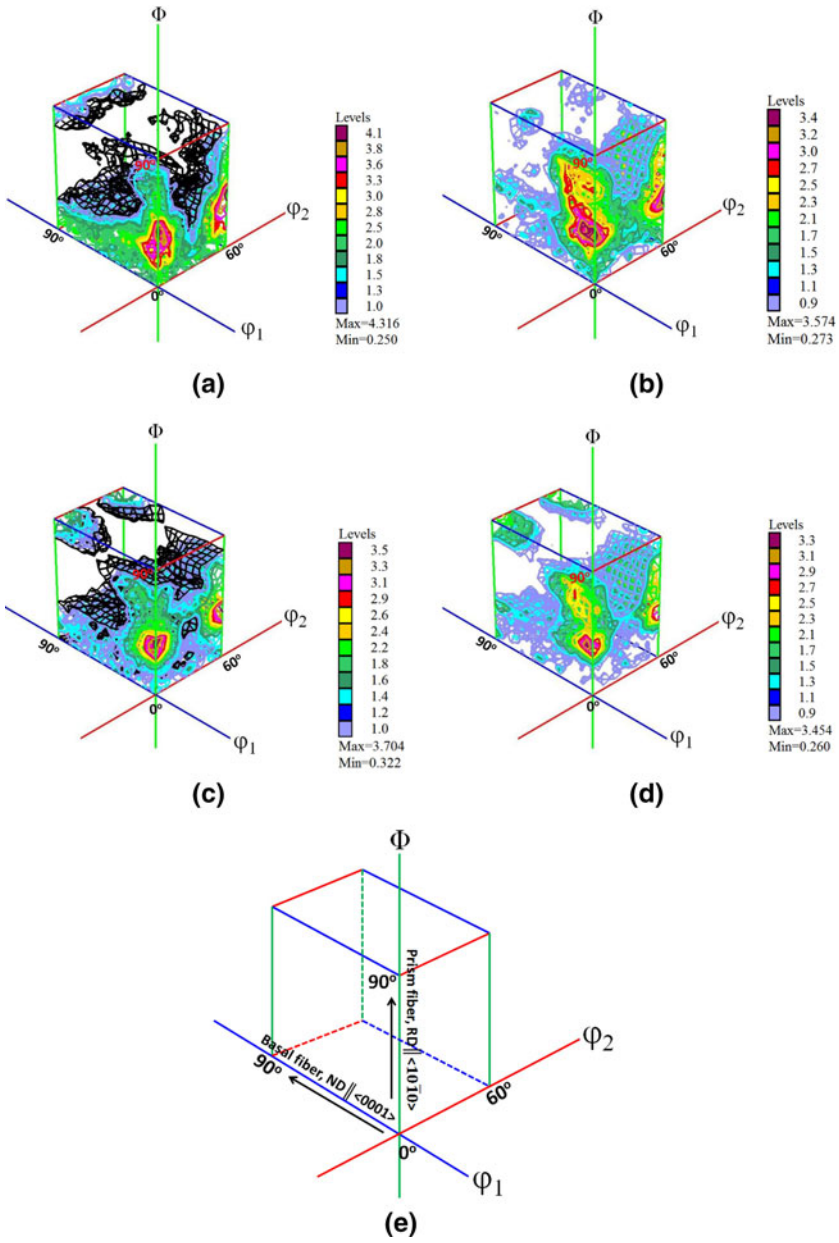

Fig. 4—Three-dimensional ODFs (Euler space) (*a*), (*b*) for Ti64 alloy after annealing for 60 min and 90 min, respectively and (*c*), (*d*) for Ti64 + B alloy after annealing for 30 min and 60 min, respectively. (*e*) Schematic indicating the location of principal texture fibers (Basal fiber with ND $\|\langle 0001\rangle$ and prism fiber with $RD\|\langle 10\bar{1}0\rangle$) in the Euler space. Color codings for the intensity levels in 3D ODFs are given alongside (For interpretation of the references to color in this figure legend, the reader is referred to the web version of this article).

Table III. Principal Texture Components in the Relevant Texture Fibers After Annealing at 1173 K (900 °C)

Alloy	Annealing Time (min)	Basal Fiber	Prism Fiber
Ti64	0	$(10\bar{1}3)[0\bar{3}31]$	$(1\bar{2}12)[10\bar{1}0]$
	60	$(10\bar{1}2)[1\bar{4}31]$	$(1\bar{2}14)[10\bar{1}0]$
	90		$(1\bar{2}15)[10\bar{1}0]$
Ti64 + B	0	$(10\bar{1}5)[4\bar{1}\bar{3}91]$	$(1\bar{2}15)[10\bar{1}0]$
	30		$(1\bar{2}14)[10\bar{1}0]$
	60		$(1\bar{2}15)[10\bar{1}0]$

Table IV. Strength, *f*(*g*), of Individual Texture Fibers in the Orientation Space at Different Annealing Conditions

Alloy	Annealing Time (min)	Basal Fiber (ND$\|\|\langle 0001\rangle$)	Prism Fiber (RD$\|\|\langle 10\bar{1}0\rangle$)
Ti64	0	4.3	2.6
	60	3.9	2.7
	90	1.4	3.1
Ti64 + B	0	2.5	1.9
	30	1.9	3.4
	60	1.3	3.7

Table V. Orientations of α Phase With Respect to the Rolling Symmetry, Corresponding Slip Systems, and Extension Directions[31,32]

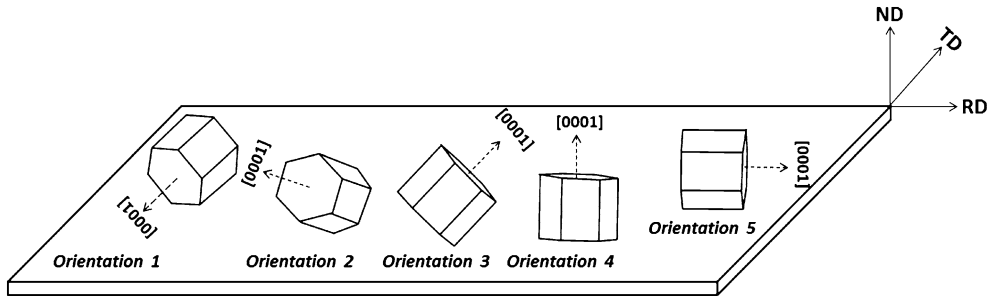

Serial Number in Top Image	Unit Cell Orientation	*c*-Axis Orientation	Possible Slip	Possible Extension	Comments
1	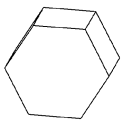	||TD	prism slip	extends to RD	very soft orientation
2		at certain angle to ND, RD, & TD	prism slip; basal slip less likely due to plain strain constraint	extends to RD	soft orientation
3		At certain angle to ND, R,D & RD	basal slip; prism slip less likely due to plain strain constraint	extends to RD	soft orientation
4	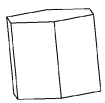	||ND	no basal slip, possibility of prism slip	may extends to RD; resists compression along ND	hard orientation
5	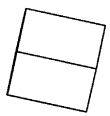	||RD	no basal slip; prism slip less likely due to plain strain constraint	no extension along RD	hard orientation

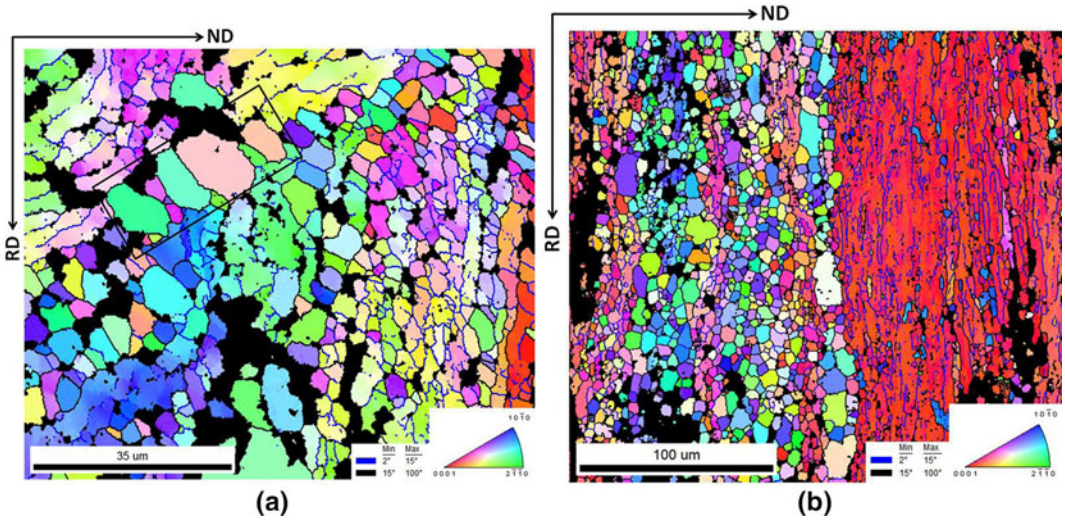

Fig. 5—Inverse pole figure (IPF) maps for Ti64 annealed up to (*a*) 30 min and (*b*) 60 min. The prior rolling directions are shown as RD (↑), ND (→), and TD pointing normal of the plane of observation. The black regions originally belongs to ($\alpha_s + \beta$) regions and separated *via* image quality criterion. Color codings showing the crystallographic orientations with respect to the principal specimen directions in the IPF maps are given alongside (For interpretation of the references to color in this figure legend, the reader is referred to the web version of this article).

promote any slip activity and are therefore inefficient for boundary formation.

As explained in Part I, most of the α colonies undergo simultaneous basal and prism slip during rolling in the Ti64 + B alloy primarily due to the weak initial texture in the as-cast condition. As a result, a large orientation gradient usually exists inside most of the α lamella of the Ti64 + B alloy when rolled at 973 K (700 °C) and leads to low angle boundary formation on annealing (Figure 7(a)). Development of sub-structural features is indicated for such an α colony in Figure 7(b) from the misorientation variation along a line inside representative α lamellae. Occasionally, point-to-point misorientation reaches ~5 to 7 deg, while point-to-origin misorientation abruptly increases by 4 to 5 deg at certain locations which correspond to sub-grain boundaries.[33] Low misorientation regions, on the other hand, are related to cell interiors with relatively fewer dislocations. It follows that the predominant fraction of α colonies is favorable to through thickness boundary formation in the Ti64 + B alloy, even for shorter annealing durations.

2. *Thermal grooving*

On rolling the Ti64 + B alloy at 1173 K (900 °C), certain dynamically recrystallized regions enclosed with high angle boundaries ($\theta \geq 90$ deg) are observed inside the large globularized α grains (discussed in Section IV–A–3 of Part I). A similar recrystallization process may occur during static annealing as well, most likely in the beginning of heat treatment. The recrystallization is related to the larger thickness of the α lamellae, which promotes sufficient strain accumulation at high temperature instead of recovery-assisted substructure formation.[8] The high angle boundaries meet the required condition for thermal grooving which is related to the interfacial diffusion of alloying elements (mostly vanadium) and controlled by the interfacial energy of the interlamellar α/α (γ_B) and interphase α/β (γ_S) boundaries.[24] In case the dihedral angle $2\phi < \pi$, (*i.e.*, $\gamma_B > \gamma_S$), the groves deepen and boundary splitting proceeds.[24–26] The splitting time of the high angle boundary is also fairly less since material transport is needed over a small distance to initiate the splitting process. The recovery-assisted low angle intralamellar α/α boundary, on the other hand, is associated with low interfacial energy and not favorable for faster thermal grooving.[23] Static recrystallization during annealing teat treatment is not likely for the Ti64 alloy, primarily due to the large aspect ratio of α lamellae. The thermal grooving thus proceeds faster in the Ti64 + B alloy wherever a high angle α/α boundary of a recrystallized region is present.

Although the small aspect ratio (large thickness) accelerates the thermal grooving due to static recrystallization in the Ti64 + B alloy, the penetration distance for the β cusps and the effective diffusion length for the alloying elements increase for thick α lamellae.[30] The thinner α lamella in the case of the Ti64 alloy, however, form intralamellar boundaries at shorter intervals due to dislocation pile up at the α/β interface.[8] The diffusion fields associated with the thermal grooving for each of these intralamellar α/α boundaries then overlap and produce constant surface curvature between them.[26] The driving force for further groove deepening, therefore, disappears and the α lamella stabilizes against boundary splitting. Such an α lamella still breaks up by high angle intralamellar α/α boundary formation due to substructure rotation and low angle boundary elimination to reduce overall boundary energy.[8] The process eventually forms "necklace"-like α grains with high angle boundaries in place of the original α lamella. One such area is marked in Figure 5(a) wherein the "necklace" structure forms in the Ti64 alloy after annealing for 15 minutes.

3. *Termination migration*

The process of termination migration is important for α lamellae where transverse boundaries are difficult to

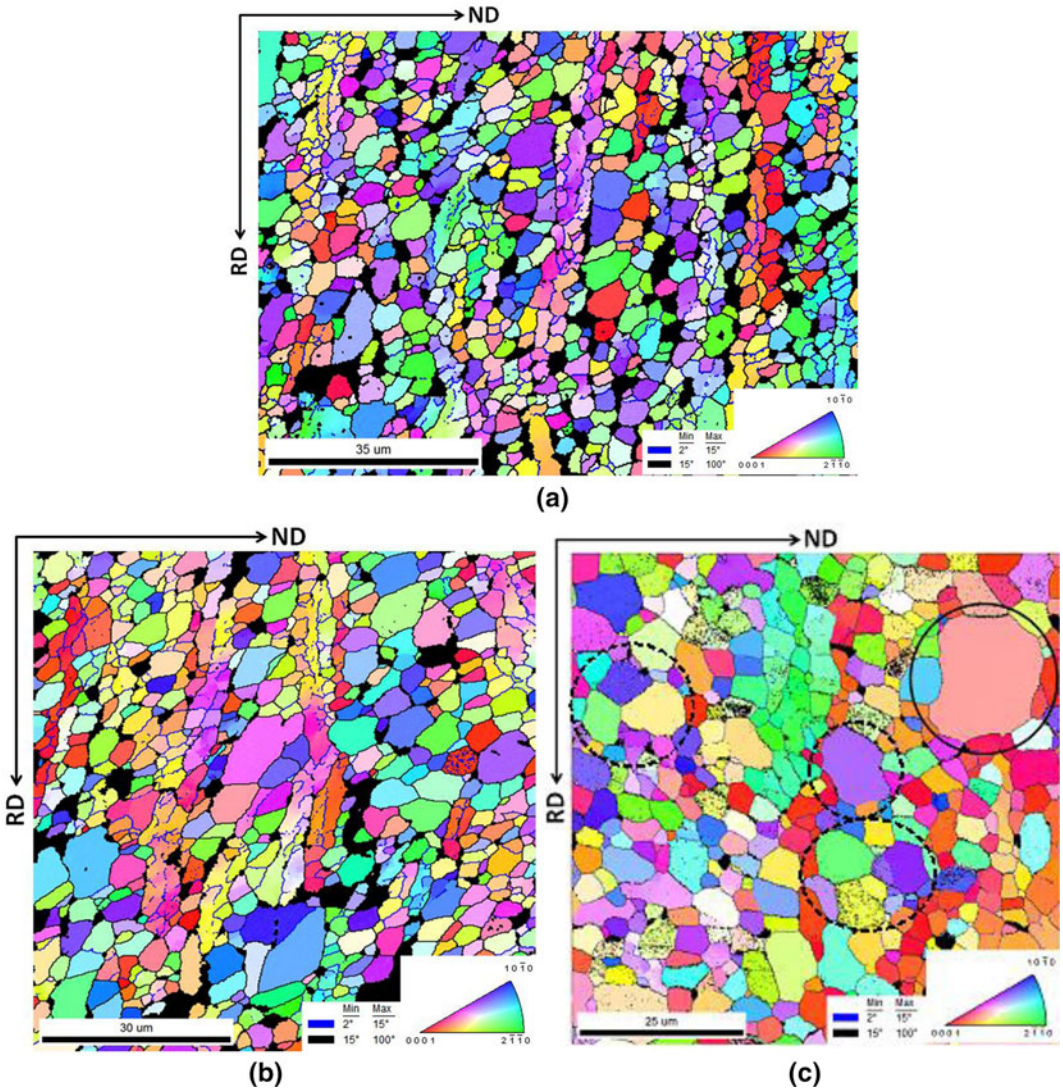

Fig. 6—Inverse pole figure (IPF) maps for Ti64 + B annealed up to (*a*) 15 min, (*b*) 30 min and (*c*) 60 min of annealing. The prior rolling directions are sown as RD (↑), ND (→) and TD pointing normal of the plane of observation. The black regions originally belongs to ($\alpha_s + \beta$) regions and separated *via* image quality criterion. Color codings showing the crystallographic orientations with respect to the principal specimen directions in the IPF maps are given alongside (For interpretation of the references to color in this figure legend, the reader is referred to the web version of this article).

form due to the starting orientation (*e.g.*, lamellae with TD||⟨0001⟩ or ND||⟨0001⟩). Moreover, the thermal grooving saturates and does not contribute to the total spheroidization process during long-term annealing since the intralamellar boundary energy decreases during prolonged thermal exposure.[23] In the absence of boundary-induced terminations, the coarsening process mainly depends on the interlamellar ends and the original α colony boundary.[27] The small α colony size and low aspect ratio of α lamellae insure a higher number of terminations in the starting (as-rolled) microstructure of the Ti64 + B alloy for such "hard" α lamellae. For the α lamellae which easily form transverse boundaries due to multiple slip (orientation 2 and 3 in Table V), the new α/β interfaces that form because of thermal grooving act as the effective terminations. The number of terminations is, therefore, always higher for the alloy Ti64 + B compared to the alloy Ti64.

4. *Cylinderization*

The process of cylinderization generally succeeds termination migration when the α lamellae are sufficiently coarsened and their aspect ratio drops below a certain critical value.[24,26] This critical aspect ratio is found to be ~3 for a TiAl/Ti_3Al two-phase lamellar alloy.[27] The microstructural features of this alloy system (alternating lamellae of TiAl and Ti_3Al) can be considered similar to that of Ti-6Al-4V. The termination migration rate, however, is not expected to be the same since vanadium diffusion is the rate-controlling factor for Ti-6Al-4V instead of Al diffusion in TiAl/Ti_3Al.[8,27] The critical aspect ratio can still be used as a primary benchmark to differentiate between the two alloys used in the present study.

The average aspect ratio drops below the critical value of 3 after 15 minutes of annealing in the Ti64 + B alloy (Figure 3(a)). On the other hand, the aspect ratio

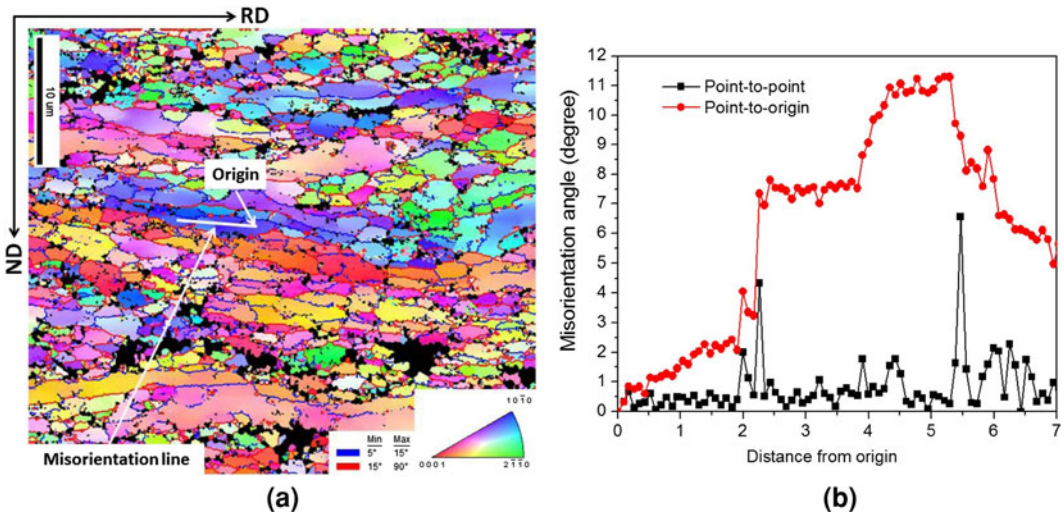

Fig. 7—(*a*) IPF map for Ti64 + B alloy rolled at 973 K (700 °C) up to 90 pct and (*b*) misorientation variation along the line shown in (a). The prior rolling directions are shown as ND (↑), RD (→), and TD pointing normal of the plane of observation. The black regions originally belongs to ($\alpha_s + \beta$) regions and separated *via* image quality criterion. Color codings showing the crystallographic orientations with respect to the principal specimen directions in the IPF maps are given alongside (For interpretation of the references to color in this figure legend, the reader is referred to the web version of this article).

remains well above 3 for the alloy Ti64 even after 60 minutes of annealing. This difference is primarily related to the starting smaller aspect ratio and ease of termination migration in the Ti64 + B alloy. The early achievement of critical aspect ratio hence facilitates coarsening by cylinderization. The coarsened cylinder can finally break and produce small equiaxed α grains by Rayleigh instability formation in case of the Ti64 + B alloy.[24] Furthermore, the presence of unsplitted low angle boundaries (due to overlapping diffusion fields during thermal grooving) in the Ti64 alloy stabilize the α lamella against cylinderization. This is because cylinderization requires an increase in the area of these α/α internal boundaries and interfacial energy continuously decreases as the α lamella cylinderizes.[26,34]

5. *Interfacial diffusion*

The interfacial coherency of α/β interphase boundary plays an important role towards the observed difference in the static annealing kinetics of the two alloys.[23–28] The α/β interface usually remains semi-coherent in the cast condition and undergoes a loss of coherency during rolling due to the breakage of Burgers relationship between the two phases.[29] This conversion increases the interfacial energy of the α/β interface and effectively accelerates the diffusion rate during processes like thermal grooving, termination migration, and cylinderization.[23] The loss of interfacial coherency is up to a lesser extent for the alloy Ti64 + B because of starting microstructural features like low aspect ratio (discussed in Section IV–A–3 of Part I). However, the TiB particles present in the Ti64 + B alloy are characterized by a highly incoherent interface with respect to both α and β phases.[35] In addition, strain accumulation occurs around these particles during rolling due to the inhomogeneous deformation response of hard particles and soft matrix.[36–38] The high interfacial energy thus associated with the TiB interfaces effectively accelerates the diffusion rate and promotes faster globularization near these particles. This is experimentally shown in the compositional maps of the Ti64 + B alloy annealed up to 60 minutes (Figure 8). The aluminum (*i.e.,* α phase) as well as vanadium (*i.e.,* β phase) distribution in the microstructure indicates that the penetration of β phase (marked in Figure 8(d)) through the α lamellae is most prominent near the TiB particles.

6. *Static coarsening for Ti64 + B Alloy*

The annealing of the alloy Ti64 + B for 60 minutes results in the formation of equiaxed α_p grains which are larger than the average globularized α_p grain size. One such grain is marked with an arrow in the inset of Figure 2(d). The IPF map obtained at this condition similarly reveals few such large equiaxed α_p grains (marked in Figure 7(c)). These grains are mostly surrounded by several small equiaxed α grains and bounded by high angle boundaries. Several possibilities exist for the formation of such coarse α_p grains. The first possibility is the coarsening of primary α grains by Ostwald ripening wherein smaller equiaxed α_p grains dissolve and coarser equiaxed α_p grains grow in order to decrease the overall interfacial area.[9,39] The coarsening process generally occurs once the aspect ratio of the primary α phase is effectively reduced by boundary splitting and smaller equiaxed α grains form in the microstructure.[5,6] The faster rate of globularization for the alloy Ti64 + B insures sufficient volume fraction of equiaxed α grains in the microstructure when the annealing is carried up to 60 minutes. Coarsening, therefore, occurs during the latter part of annealing.

The second possibility involves epitaxial growth of the primary α grains due to the large super-saturation

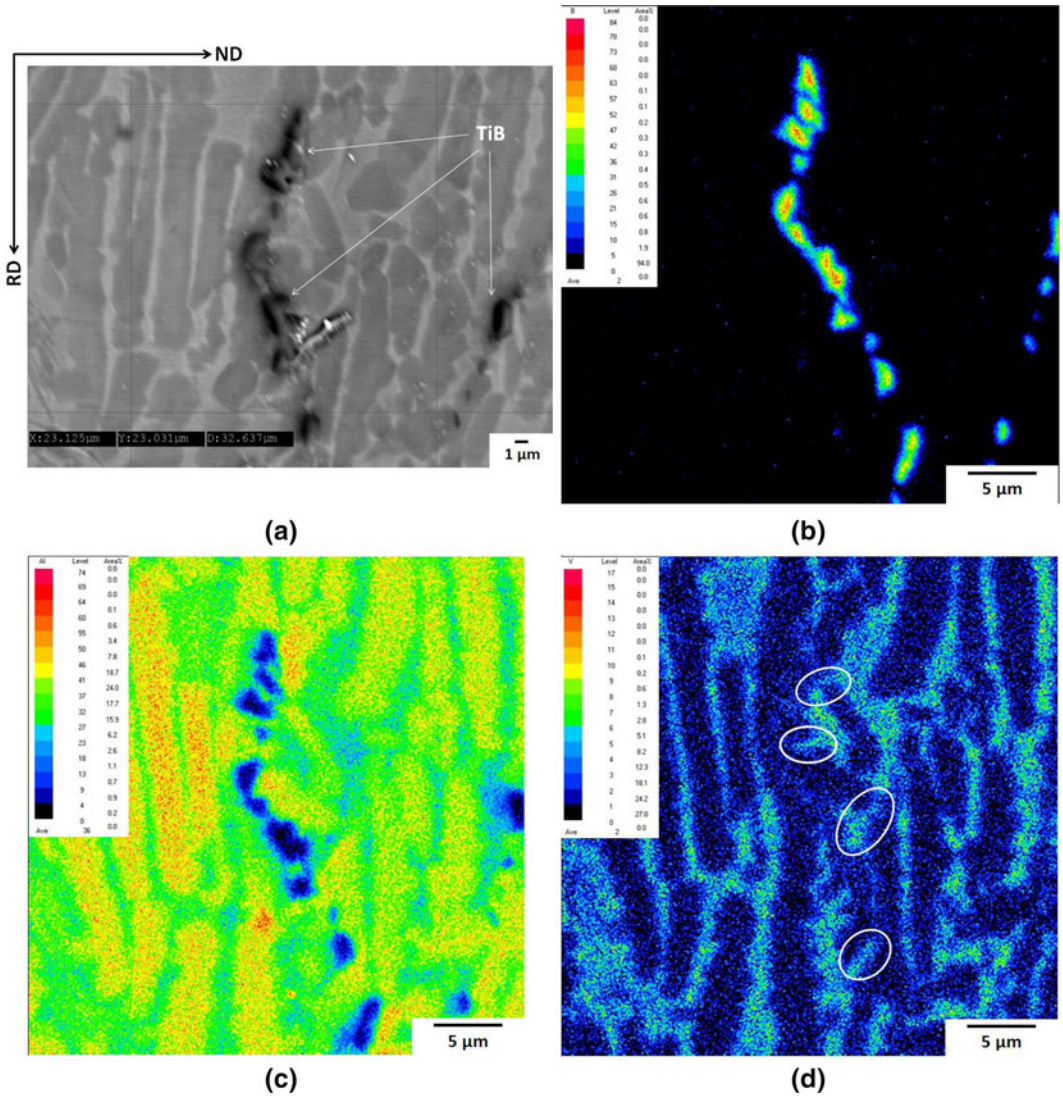

Fig. 8—(*a*) BSE micrograph from Ti64 + B alloy annealed up to 60 min showing the area of EPMA scan and (*b*) through (*d*) compositional maps showing the distribution of boron, aluminum, and vanadium, respectively, in the microstructure. The color coding for the compositional maps is given alongside. The prior rolling directions are shown in (a) as RD (↑), ND (→), and TD pointing normal of the plane of observation (For interpretation of the references to color in this figure legend, the reader is referred to the web version of this article).

present in the β matrix during cooling from the annealing temperature.[7] The primary α grain growth is stopped once the secondary lamellar α phase starts forming inside the β phase which effectively pins down the α_p grain growth and reduces the super-saturation of the β matrix. The temperature at which secondary α forms is, however, found to reduce with increasing cooling rate.[7] The air cooling (cooling rate ~3 °C/s), as employed in the present investigation, is sufficient to retard the α_s colony formation, and α_p grain growth can occur up to a much lower temperature [~973 K (700 °C)] for the Ti64 + B alloy.

It is important to note that the coarsening rate generally follows r^3 *vs* t (r = radius of α_p grains after time t) kinetics. This means even a smaller duration, either during the latter period of annealing or during cooling, is sufficient to produce significant growth of globularized α_p grains.[27] The coarsening is most pronounced for the alloy Ti64 + B after 60 minutes of annealing since only for this condition, the microstructure mostly consists of equiaxed α_p grains at the beginning of coarsening.

B. *Texture Evolution*

The texture evolution during annealing reveals that the basal fiber (ND||⟨0001⟩) weakens and the prism fiber $(RD\|\langle 10\bar{1}0\rangle)$ strengthens upon annealing for both the alloys (Table IV).

1. *Role of $\alpha \rightarrow \beta \rightarrow \alpha$ phase transformation*

At the annealing temperature of 1173 K (900 °C), the microstructure contains (~34 ± 2) pct β phase for the alloy Ti64 and (~39 ± 1.7) pct for the alloy Ti64 + B (Table II). The overall texture is thus largely affected by the variant selection during $\alpha \rightarrow \beta \rightarrow \alpha$ transformation

process.[12–18,40–42] The two-way transformation favors certain α variants during the forward ($\alpha \rightarrow \beta$) transformation and certain other α variants during reverse ($\beta \rightarrow \alpha$) transformation; more often such α variants are related by a 90 deg misorientation.[31] The $\alpha \rightarrow \beta \rightarrow \alpha$ transformation texture generally modifies the prior rolling texture significantly during ($\alpha + \beta$) annealing since variant selection is more probable at two-phase regions compared to single-phase β processing.[34] The secondary α phase generally maintains a close orientation

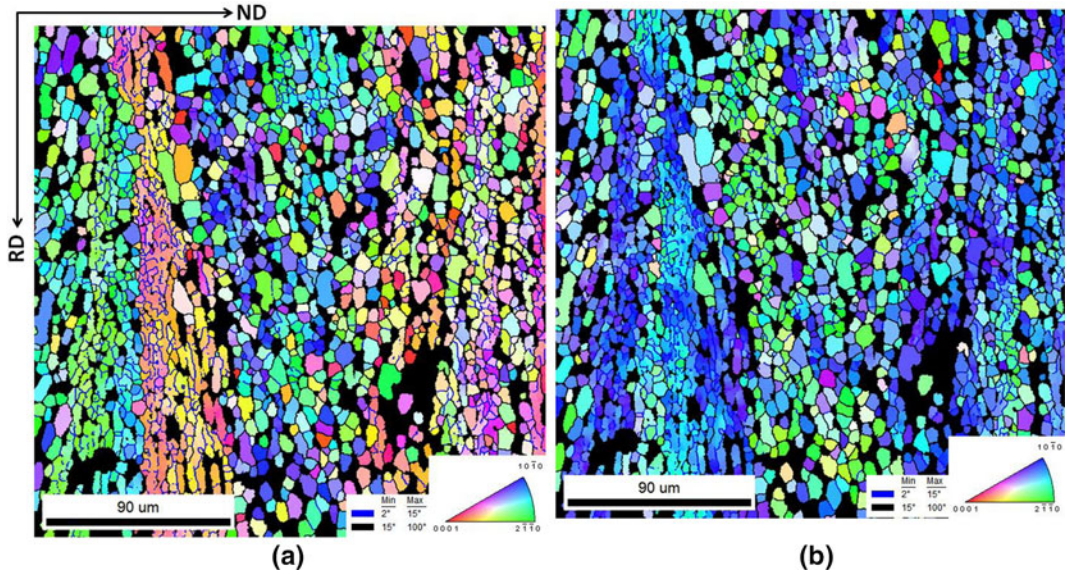

Fig. 9—Inverse pole figure (IPF) maps for Ti64 after 90 min of annealing with principal directions (*a*) TD and (*b*) RD pointing normal of the plane of observation. Low angle ($\theta < 15$ deg) and high angle ($\theta > 15$ deg) boundaries are colored in blue and black, respectively. The black regions originally belongs to ($\alpha_s + \beta$) regions and separated *via* image quality criterion. Color codings showing the crystallographic orientations with respect to the principal specimen directions in the IPF maps are given alongside (For interpretation of the references to color in this figure legend, the reader is referred to the web version of this article).

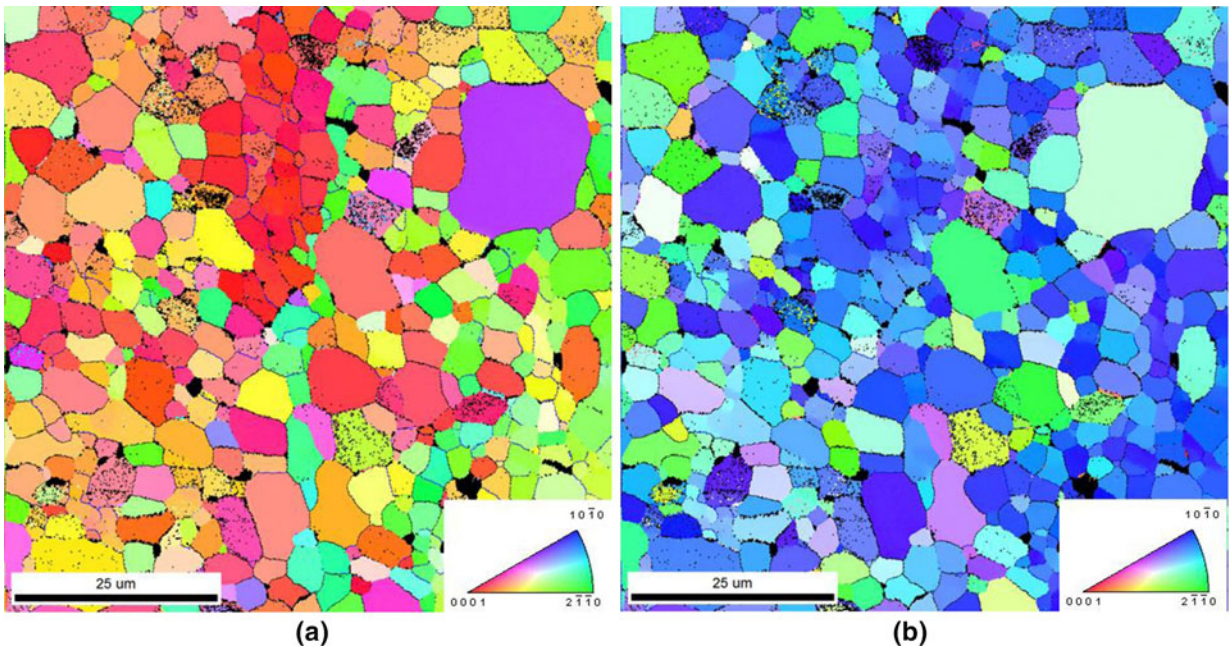

Fig. 10—Inverse pole figure (IPF) maps for Ti64 + B after 60 min of annealing with principal directions shown as (*a*) ND and (*b*) RD pointing normal of the plane of observation. Low angle ($\theta < 15$ deg) and high angle ($\theta > 15$ deg) boundaries are colored in blue and black, respectively. The black regions originally belong to ($\alpha_s + \beta$) regions and separated *via* image quality criterion. Color codings showing the crystallographic orientations with respect to the principal specimen directions in the IPF maps are given alongside (For interpretation of the references to color in this figure legend, the reader is referred to the web version of this article).

to the primary α phase in order to reduce the elastic (transformation) strain energy at the α_p/prior β phase boundary.[43–45] In the case of α colonies with orientations 1, 4, and 5 (Table V), globularization is sufficiently retarded during annealing. Out of these three "passive" orientations, the α colonies with orientation 4 belong to the basal fiber (ND||⟨0001⟩). On the other hand, α colonies with orientation 2 and 3 globularize much faster due to the ease of boundary splitting. As shown in Figure 9, these globularized α colonies primarily belong to the prism fiber $RD\|\langle 10\bar{1}0\rangle$.

During the early stages of annealing, globularized α_p grains quickly form a dislocation substructure and become sufficiently strain free. Easy prism slip for the straight α colonies (with TD||⟨0001⟩ initial orientation) similarly leads to a strain-free condition. The α colonies with orientation 4 (Table V) which are part of the basal fiber, on the other hand, possess combatively more strain. These α colonies, therefore, preferentially transform to β phase at the start of annealing.[34] When the reverse $\beta \rightarrow \alpha$ transformation takes place during cooling, the secondary α colonies follow the orientation of the globularized primary α grains and also form with $RD\|\langle 10\bar{1}0\rangle$ orientations. The net result is, therefore, the strengthening of prism fiber and weakening of basal fiber after annealing.

2. *Preferential primary α grain growth*

A secondary source of texture evolution during annealing can be the preferential growth of certain primary α grains during coarsening *via* Ostwald ripening.[46] The α colonies which belongs to $RD\|\langle 10\bar{1}0\rangle$ fiber globularize much faster and therefore possess a growth advantage over other unfavorably oriented primary α grains. The remnant α colonies or small globularized α grains then dissolve during prolonged annealing and epitaxial growth occurs for the large existing globularized primary α grains. This condition is effectively met in the Ti64 + B alloy after 60 minutes of annealing. The IPF maps in Figures 10(a) and (b) show that many of the coarse α_p grains (marked in Figure 6(c)) in this annealed specimen belong to the prism fiber. The coarsest grain in the microstructure (marked with solid circle in Figure 6(c)), however, retains an orientation such that c-axis is inclined to the three principal prior rolling directions. Since this orientation is favorable for the earliest globularization, growth advantage possibly dominates over orientation factor. It suggests that the α texture modification by preferential growth may not be as effective as the strong variant selection during $\alpha \rightarrow \beta \rightarrow \alpha$ transformation.

V. CONCLUSIONS

In the present study, the evolution of microstructure and texture during sub-transus isothermal annealing of warm-rolled Ti-6Al-4V and Ti-6Al-4V-0.1B alloys has been investigated. The salient outcomes of the study are the following:

- The globularization kinetics is faster in the case of the Ti-6Al-4V-0.1B alloy compared to the control Ti-6Al-4V alloy under identical annealing conditions. This difference is attributed to the presence of α lamellae favorably oriented for multiple slip during prior rolling that facilitates easy boundary splitting during subsequent annealing.
- The morphological conversion mechanisms like termination migration and cylinderization initiate early in Ti-6Al-4V-0.1B alloy compared to the control Ti-6Al-4V alloy due to the smaller α colony size, lower aspect ratio of α lamellae, and the presence of TiB particles in the former.
- The static coarsening of primary α grains (α_p) occurs *via* Ostwald ripening during long-term annealing of the Ti-6Al-4V-0.1B alloy. Epitaxial growth of such α_p grains during cooling is an additional possibility.
- Texture modification due to annealing manifests in the weakening of basal fiber (ND||⟨0001⟩) and strengthening of prism fiber ($RD\|\langle 10\bar{1}0\rangle$) compared to the as-rolled conditions for both the alloys. This occurs as a result of variant selection in $\alpha \rightarrow \beta \rightarrow \alpha$ transformation during secondary α formation.

To conclude, the first part of the present study revealed that the boron-modified alloy can be successfully rolled at relatively lower temperature (in "warm" processing regime) compared to Ti-6Al-4V without any macroscopic or microscopic defects. In the second part, it has been realized that the sub-transus annealing of warm-rolled specimens leads to faster microstructural conversion from lamellar to equiaxed α morphology for the boron-modified alloy under identical static annealing conditions. Together with the superior rolling response of the Ti-6Al-6V-0.1B alloy, an efficient processing schedule involving lesser temperature and time can be designed.

ACKNOWLEDGMENTS

The authors acknowledge the Institute Nanoscience Initiative (INI) and Institute X-ray Facility at the Indian Institute of Science, Bangalore, India, and the National facility for orientation imaging microscopy and X-ray bulk texture at the Indian Institute of Technology Bombay for providing the required research facilities. The materials used for the study were originally provided by Dr. Dan Miracle of AFRL and Dr. S. Tamirisakandala of FMW Composites. The authors are thankful to Mr. Nataraj B.R., Mr. Ashranth, Mr. Atanu Chowdhury, and Mr. Nachiketa Ray for microstructural measurements.

REFERENCES

1. S. Roy and S. Suwas: *Metall. Mater. Trans A*, 2013. DOI: 10.1007/s11661-013-1672-4.
2. G. Lütjering: *Mater. Sci. Eng., A*, 1998, vol. 243, pp. 32–45.
3. G. Lütjering: *Mater. Sc. Eng. A*, 1999, vol. 263, pp. 117–26.
4. M. Peters, G. Lütjering, and G. Ziegler: *Z. Metallkd.*, 1983, vol. 74, pp. 274–82.
5. N. Stefansson, S.L. Semiatin, and D. Eylon: *Metall. Mater. Trans. A*, 2002, vol. 33A, pp. 3527–34.

6. N. Stefansson and S.L. Semiatin: *Metall. Mater. Trans. A*, 2003, vol. 34A, pp. 691–98.
7. S.L. Semiatin, S.L. Knisley, P.N. Fagin, D.R. Barker, and F. Zhang: *Metall. Mater. Trans. A*, 2003, vol. 34A, pp. 2377–86.
8. I. Weiss, F.H. Froes, D. Eylon, and G.E. Welsch: *Metall. Trans. A*, 1985, vol. 17A, pp. 1935–47.
9. S.L. Semiatin, B.C. Kirby, and G.A. Salishchev: *Metall. Mater. Trans. A*, 2004, vol. 35A, pp. 2809–19.
10. R.L. Fullman: *J. Met*., 1993, vol. 3, pp. 447–52.
11. S.L. Semiatin, V. Seetharaman, and I. Weiss: *Mater. Sci. Eng., A*, 1999, vol. 263, pp. 257–71.
12. S. Suwas and A.K. Singh: *Mater. Sci. Eng., A*, 2003, vol. 355, pp. 331–37.
13. S. Suwas and A.K. Sing: *Metal. Mater. Trans. A*, 2004, vol. 35A, pp. 925–38.
14. S. Suwas, R.K. Ray, A.K. Singh, and S. Bhargava: *Acta Mater*., 1999, vol. 47, pp. 4585–98.
15. S. Suwas, A.K. Singh, R.K. Ray, and S. Bhargava: *Scripta Mater*., 1996, vol. 35, pp. 897–02.
16. S. Suwas and R.K. Ray: *Acta Mater*., 1999, vol. 47, pp. 4599–14.
17. N.P. Gurao, A.A. Ali, and S. Suwas: *Mater. Sc. Eng. A*, 2009, vol. 504, pp. 24–35.
18. H. Inagaki: *Z. Metallkunde*, 1990, vol. 81, pp. 433–45.
19. S. Roy, S. Suwas, S. Tamirisakandala, D.B. Miracle, and R. Srinivasan: *Acta Mater*., 2011, vol. 59, pp. 5494–510.
20. S. Roy, V. Tungla, and S. Suwas: *Metall. Mater. Trans. A*, 2011, vol. 42A, pp. 2535–41.
21. S. Roy and S. Suwas: *Mater. Sc. Eng. A*, 2012, vol. 540, pp. 152–63.
22. S. Roy and S. Suwas: *J. Alloys Compd*., 2013, vol. 548, pp. 110–25.
23. S. Zherebtsov, M. Murzinova, G. Salishchev, and S.L. Semiatin: *Acta Mater*., 2011, vol. 59, pp. 4138–50.
24. G. Sharma, R.V. Ramanujan, and G.P. Tiwari: *Acta Mater*., 2000, vol. 48, pp. 875–89.
25. Y.L. Tian and R.W. Kraft: *Metall. Trans. A*, 1987, vol. 18A, pp. 1403–14.
26. J.C.M. Kampe, T.H. Courtney, and Y. Leng: *Acta Metall*., 1989, vol. 37, pp. 1735–45.
27. M.F. Bartholomeusz and J.A. Wert: *Metall. Mater. Trans. A*, 1994, vol. 25A, pp. 2371–81.
28. T.H. Courtney and J.C.M. Kampe: *Acta Metall*., 1989, vol. 37, pp. 1747–58.
29. S. Mironov, M. Murzinova, S. Zherebtsov, G.A. Salishchev, and S.L. Semiatin: *Acta Mater*., 2009, vol. 57, pp. 2470–81.
30. S.L Semiatin and T.R Bieler: *Acta Mater*., 2001, vol. 49, pp. 3565–73.
31. T.R. Bieler and S.L. Semiatin: *Inter. J. Plast*., 2002, vol. 18, pp. 1165–89.
32. T.R. Bieler, M.G. Glavicic, and S.L. Semiatin: *J. Metals*, 2002, vol. 54, pp. 31–36.
33. F. Cao, E.K. Cerreta, C.P. Trujillo, and G.T. Gray, III: *Acta Mater*., 2008, vol. 56, pp. 5804–17.
34. L. Zeng and T.R. Bieler: *Mater. Sci. Eng., A*, 2005, vol. 392, pp. 403–14.
35. H. Feng, Y. Zhou, D. Jia, and Q. Meng: *Scripta Mater*., 2006, vol. 55, pp. 667–70.
36. S. Roy, A. Sarkar, and S. Suwas: *Mater. Sci. Eng., A*, 2010, vol. 528, pp. 449–58.
37. A. Sarkar, S. Roy, and S. Suwas: *Mater. Charact*., 2011, vol. 62, pp. 35–42.
38. S. Roy, S. Suwas, S. Tamirisakandala, R. Srinivasan, and D.B. Miracle: *Suppl. Proc. TMS*, 2009, vol. 3, pp. 63–70.
39. S.L. Semiatin, N. Stefansson, and R.D. Doherty: *Metall. Mater. Trans. A*, 2005, vol. 36A, pp. 1372–76.
40. M. Peters and G. Luetjering: *Titanium 80,* H. Kimura, O. Izumi, Eds., Metallurgical Society of AIME, 1980, pp. 925–38.
41. Z.S. Zhu, J.L. Gu, and N.P. Chen: *Scripta Mater*., 1996, vol. 34, pp. 1281–86.
42. A.W. Bowen: *Mater. Sci. Eng., A*, 1977, vol. 29, pp. 19–28.
43. L. Germain, N. Gey, M. Humbert, P. Vo, M. Jahazi, and P. Bocher: *Acta Mater*., 2008, vol. 56, pp. 4298–4308.
44. M. Humbert, L. Germain, N. Gey, P. Bocher, and M. Jahazi: *Mater. Sci. Eng., A*, 2006, vol. 430, pp. 157–64.
45. L. Germain, N. Gey, M. Humbert, P. Bocher, and M. Jahazi: *Acta Mater*., 2005, vol. 53, pp. 3535–43.
46. A.A. Salem, M.G. Glavicic, and S.L. Semiatin: *Mater. Sci. Eng., A*, 2008, vol. 494, pp. 350–59.